CrossMark

The mechanism study on the cooperative flame resistance effect between HMP and NP in ABS by TG–FTIR

Zhiyi Yang[1] · Zhanyong Gu[1] · Xiushan Yang[1] · Zhiye Zhang[1] · Xinlong Wang[1] · Xiaodong Chen[1] · Lin Yang[1]

Abstract Thermogravimetry (TG) coupled with Fourier transform infrared spectroscopy (FTIR) (TG–FTIR) is an effective tool on studying the mechanism of the flame retardant. The mechanism on the cooperative effect between hydroquinone bis(di-2-methylphenyl phosphate) (HMP), which is an effective flame retardant, and novolac phenol (NP) in acrylonitrile–butadiene–styrene (ABS) is investigated by TG–FTIR under air in this study. The TG–FTIR of ABS/HMP, ABS/HMP/NP and ABS/NP are discussed carefully as well as their semi-quantitative analyses. The semi-quantitative analysis results of TG–FTIR show that ABS/HMP, ABS/HMP/NP and ABS/NP decompose in a two-step process. The first step is mainly the process of thermal degradation, macromolecules being decomposed into micromolecules containing many functional groups such as C_{Ar}–H, –CH_2–, –OH, P–O–C_{Ar}. The second step is mainly the process of combustion, the layer of carbon being further oxidized into carbon dioxide, water and alkyne. The residue of ABS/HMP/NP is the highest as well as its temperature at which the maximum of mass loss rate occurs. Furthermore, the comparison of their semi-quantitative analyses indicates that NP could absorb parts of micromolecules containing the functional groups of –OH, CH_2– and C_{Ar}–H, contributing to the formation of carbon layer, and HMP slows down the degradation of the carbon layer, achieving the cooperative effect.

Keywords TG–FTIR · Mechanism · Cooperative flame

✉ Lin Yang
  18980632893@163.com

1 School of Chemical Engineering of Sichuan University, Chengdu 610065, Sichuan, China

Introduction

ABS is a widely used thermoplastic material as a result of its good mechanical and physical properties, chemical resistance and processing advantages [1–4]. However, ABS is highly flammable owing to its chemical constitution, which limits its application in a lot of fields. Therefore, fire retardation is important and necessary for this material [5].

NP has acquired unique applications in a number of polymer systems, and a lot of studies have been done to examine the properties of NP [6–8]. NP has been used to delay the volatilization of the degradation products of phosphorous-based flame retardants [8]. NP is a very promising material as a result of char formers consisting of a relatively robust aromatic backbone and polar hydroxyl functionalities [6].

As an organic flame retardant, HMP has good compatibility with ABS. Meanwhile, it is halogen-free flame retardant which is environmentally friendly. Many phosphorus-based flame retardants, such as resorcinol bis(diphenyl phosphate) (RDP) [9, 10] and bisphenol A bis(diphenyl phosphate) (BDP) [11], have been employed as flame retardants for ABS resins with NP. However, most organic phosphorus-based flame retardants used for ABS are liquid, which is not convenient during the manufacture of flame-retarded products [12]. The melting point of HMP is about 78 °C, which facilitates later processing [3]. The decomposition of HMP process began at 378 °C (around that of ABS) (374 °C), which indicates that HMP can play a better fire role in the process of thermal decomposition [3]. Owing to that NP has the extremely strong ability of forming carbon and HMP makes carbon layer more hard, the ABS/HMP/NP gains good flame-retardant performance [3, 13]. The thermal degradation mechanism of HMP has been successfully studied by TG–FTIR [14]. TG–FTIR is

an effective tool on studying the degradation products [15]. The TG curve provides the degradation process of composites, and at the same time, the FTIR spectra identify the degradation products of the evolved gases in the process of degradation. Although TG is used widely in thermal analyses study, the composition of evolved gas in the process of degradation cannot be identified and analyzed only by TG. FTIR analyses can identify functional groups as well as elemental composition. On the other hand, FTIR results can be used to identify the functional groups generated in the process of degradation [16]. In other words, FTIR, providing lots of information on mixed gases with functional groups, can be used to analyze the composition of mixture and evaluate some gaseous substances [17]. TG is used widely in thermal analyses study under N_2. But in order to simulate the process of combustion, TG–FTIR is used to study thermal degradation mechanism and the cooperative effect between HMP and NP in ABS under air.

The flame-retardant mechanism of ABS/HMP/NP composites is much more complicated as a result of its structure and composition. Considering the composition of evolved gas in the process of degradation can be observed and these gas can be analyzed online, TG–FTIR has already been used widely to study biomass pyrolysis [15, 18] and polymers thermal degradation [19, 20], as well as to examine the gas which is hazardous that may be generated in the process of thermal degradation.

In this study, evolved gases from the process of thermal degradation during TG–FTIR experiment were swept into gas cell immediately by carrier gas. The results of TG and composition of evolved gases obtained through the study provide a lot of information to understand the pyrolysis characteristics of ABS/HMP, ABS/HMP/NP and ABS/NP composites. The results of TG–FTIR indicate that there exists the cooperative effect between HMP and NP in ABS.

Experimental

Materials

ABS (PA-709) was provided by Qi Mei industrial Co., Ltd. (China). NP (2123 MA) was provided by Heng Xin Chemical Reagent Co., Ltd. (China). HMP was synthesized with phosphorus oxychloride, hydroquinone and 2-methylphenol in our laboratory [3].

Sample preparation

Before melt blending, all the components are dried in a vacuum oven at 80 °C for 2 h. The composites of ABS, with HMP and NP, are prepared in a Huck mixer at a temperature of about 190 °C and then molded into plates

with a thickness of 3 mm. Table 1 shows the compositions of ABS/HMP, ABS/HMP/NP and ABS/NP as well as their results of LOI and UL-94.

Measurements

TG–FTIR analyses of ABS/HMP, ABS/HMP/NP and ABS/NP were performed using a TGA 851 thermogravimetric analyzer interfaced with a Nicolet IS10 FTIR spectrometer. The three samples are placed in different aluminum crucibles in sequence and heated from 50 to 800 °C (10 °C min^{-1}) under air in the same experiments (flow rate = 30 mL min^{-1}). The pyrolysis gas products are transferred to the FTIR spectrometer in the degradation process via a metal pipe (200 °C to avoid condensation).

Results and discussion

TG and DTG analyses

Figure 1 shows the TG and DTG curves for ABS/HMP, ABS/HMP/NP and ABS/NP under air. The TG and DTG curves indicate that all of the three composites decompose in two steps. The first step occurs from 327 to 477 °C, and the second step occurs from 527 to 627 °C. The mass in the first step reduces much more than that in the second step. The decomposition of ABS/HMP/NP in first step follows a similar trend to the decomposition of ABS/NP and is slower than the decomposition of ABS/HMP. Meanwhile, ABS/HMP/NP decomposes much slower than ABS/NP and the residue of ABS/HMP/NP is the highest.

The TG and DTG curves are summarized in Table 2. Not only T_{1onset} of the three samples in this article is similar to the T_{onset}^* of Ren [3], but also T_{1max} is similar to T_{max}^*. It is probably because the first degradation step is mainly thermal degradation and only a little oxygen participates in the reaction. The tiny difference is probably owing to the difference of the TG instruments and gas environment. These three samples in this article have T_{2onset}, while Yan-yan Ren's have not, which is assigned to the process of combustion under air in the second degradation step in this test.

Table 1 Results of LOI and UL-94 tests

Sample	Components/mass%			LOI1	UL-94
	ABS	HMP	NP		
ABS/HMP	70	30	0	24.9	Failed
ABS/HMP/NP	70	20	10	33.5	V-1
ABS/NP	70	0	30	22.2	Failed

The first degradation process of ABS/HMP/NP begins at 382 °C, which is higher than that of ABS/HMP (365 °C) and ABS/NP (377 °C). In the first step, the temperature with
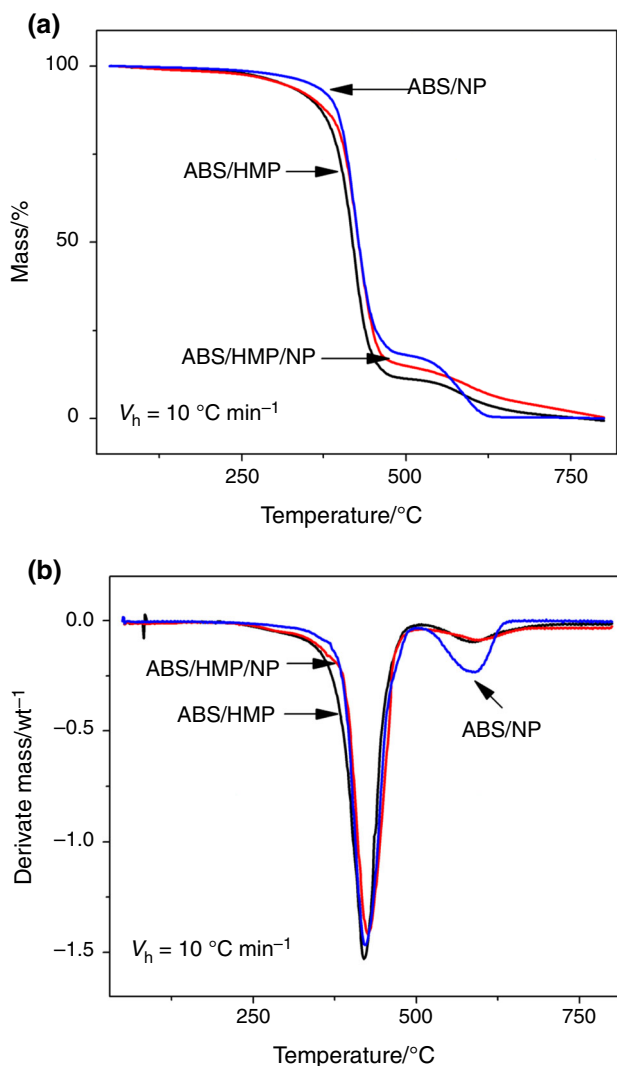

Fig. 1 TG and DTG curves of ABS/HMP, ABS/HMP/NP and ABS/NP under air (**a** TG, **b** DTG)

the maximum mass loss rate of ABS/HMP/NP is 426 °C, which is a little higher than that of ABS/HMP (420 °C) and ABS/NP (422 °C). The maximum mass loss rate of ABS/HMP/NP is 1.38% °C^{-1}, which is a little lower than that of ABS/HMP (1.41% °C^{-1}) and ABS/NP (1.50% K^{-1}). The second degradation process of ABS/HMP/NP begins at 542 °C, which is higher than that of ABS/HMP (530 °C) and ABS/NP (527 °C). In the second degradation process, the maximum mass loss rate of ABS/NP is 0.25% °C^{-1}, which is much higher than that of ABS/HMP (0.10% °C^{-1}) and ABS/HMP/NP (0.09% °C^{-1}). When the second step ends, the remaining residue of ABS/HMP/NP is 7.0%, which is higher than that of ABS/HMP (3.7%) and ABS/HMP/NP (0.6%). All of these indicate that HMP and NP exhibit cooperative effect in ABS. NP plays an important role in the first decomposition step, and HMP plays an important role in the second decomposition step.

FTIR analyses

In Fig. 2, the FTIR gas-phase spectra are generated by the absorption bands of small molecules produced by the degradation of the composites, and characteristic absorbances are assigned in Table 3. C_{Ar}–H stretching vibrations are at 3075 and 3033 cm^{-1}, and deformation vibrations of the aromatic ring of C_{Ar}–H are at 914, 767 and 695 cm^{-1}. Accordingly, the FTIR gas-phase spectra show some peaks at wave number of 1720 cm^{-1} (C=O carboxyl stretching vibration) and 1600 cm^{-1} (C=C in aromatic ring) [7, 21]. The –CH$_2$– group is also detected at 2937 and 2874 cm^{-1} [7, 22–24], and the –OH group at 3600–3800 cm^{-1} [25]. The free water-peaks are at about 3750 cm^{-1}. The characteristic vibrations of the aromatic phosphate ester are also visible, with the phosphate group P–O–C_{Ar} at 968, 1038 and 1170 cm^{-1} (i.e., 968 cm^{-1} for the P–O–C_{Ar} stretching vibration of pentavalent phosphorus and 1170 cm^{-1} for the C–O stretching vibration) [23–26]. The absorption of P=O (1315 cm^{-1}) stretching in newly generated O=P–OH bond has appeared at 1215 cm^{-1} [27].

Table 2 Characteristic parameters of pyrolysis

Sample code	T_{1onset}/°C	$T_{1onset}*$/°C	T_{1max}/°C	MLR$_1$/% °C^{-1}	$T_{1max}*$/°C	T_{2onset}/°C	T_{2max}/°C	MLR$_2$/% °C^{-1}	Residue/ %
1	365	374	420	1.41	418	530	589	0.10	3.7
2	382	394	426	1.38	419	542	600	0.09	7.0
3	377	375	422	1.50	410	527	595	0.25	0.6

1 ABS/HMP/NP; 2 ABS/HMP/NP; 3 ABS/NP

$T*_{onset}$ and T^*_{max} are from Ren [3]

T_{1onset}, the measured temperature at which the mass loss rate began to grow rapidly in first step; T^*_{onset}, the temperature at which the mass loss rate began to grow rapidly under N$_2$; T_{1max}, the measured temperature at which the maximum of mass loss rate took place in first step; T^*_{max}, the measured temperature at which the maximum of mass loss rate took place under N$_2$; MLR$_1$, the maximum mass loss rate in the first step; T_{2onset}, the measured temperature at which the mass loss rate began to grow rapidly in second step; T_{2max}, the measured temperature at which the maximum of mass loss rate took place in second step; MLR$_2$, the maximum mass loss rate in the second step
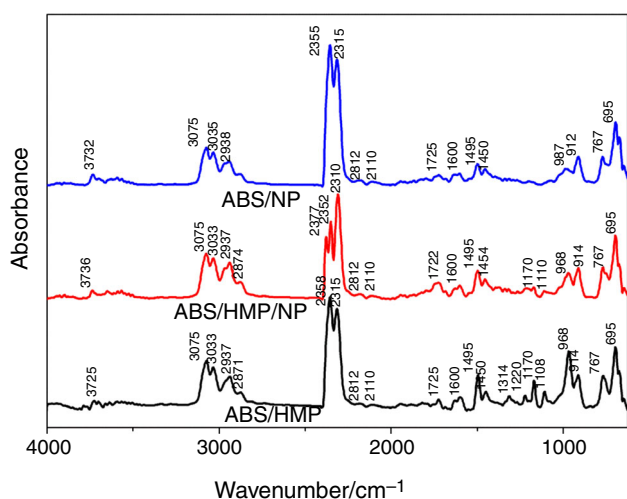
Fig. 2 FTIR spectra of pyrolysis products for ABS/HMP, ABS/HMP/NP and ABS/NP at a 350 °C

Some small molecular gaseous products are also released, including water (the successive peaks from 3400 to 4000 cm^{-1} and from 1200 to 2100 cm^{-1}) [28], carbon dioxide (from 2265 to 2400 cm^{-1}) [29] and alkyne (2182 and 2110 cm^{-1}) [14]. In order to study the mechanism of the degradation of ABS/HMP, ABS/HMP/NP and ABS/NP, they should be analyzed, respectively.

FTIR analyses of ABS/HMP

Figure 3a shows the three-dimensional (3D) FTIR spectrum for the gases produced during the thermal degradation of ABS/HMP under air. Most of the peaks appear at

Table 3 FTIR spectra band assignments

| Observed wave number/cm^{-1}	Functional group
3500-3800	–OH
3075, 3033	C_{Ar}–H stretching vibrations
2938, 2937	–CH_2– stretching vibration
2874, 2871	–CH_2– stretching vibration of
2265-2400	Carbon dioxide
2812, 2110	Alkane
1725, 1722	C=O stretch
1600	C=C aromatic ring
1315, 1314	P=O stretching
1220, 1215	O=P–OH
1170	C–O stretching vibration
968	P–O–C stretching vibration of pentavalent phosphorus
914, 912	C–H deformation vibration
767	C–H deformation vibration
695	Ring bend
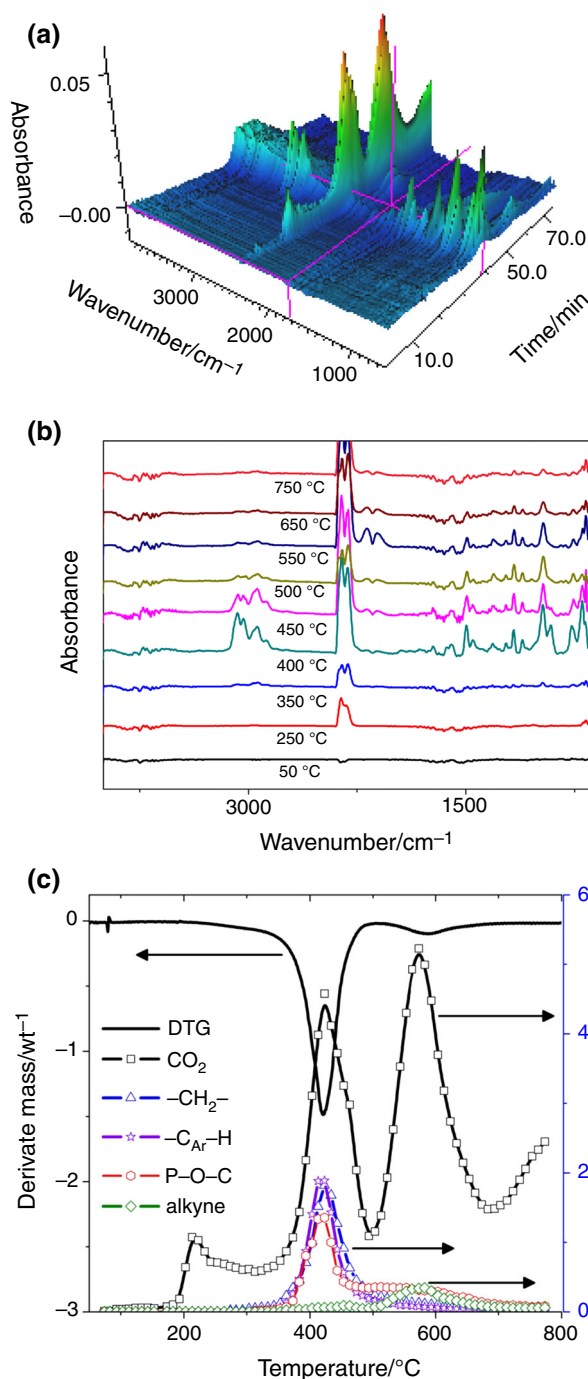
Fig. 3 FTIR spectra of ABS/HMP (a three-dimensional diagram corresponding to gases evolved from degradation under air, b FTIR spectra of pyrolysis products of different temperatures under air and c functional group's peak area at different temperatures)

35–45 min (400–500 °C), while several peaks appear at about 50 min (550 °C). So ABS/HMP decomposes in a two-step process.

Figure 3b shows the FTIR of ABS/HMP at different temperatures under air. The curve of FTIR has no peaks but the peak of CO_2 before 623 K, which indicates there is

little decomposition before 350 °C. From 400 to 450 °C, there are a lot of peaks representing the functional groups such as C_{Ar}–H, –CH_2–, P–O–C_{Ar}, P=O, CO_2, –OH and C=C, which indicates that the composite begins to decompose rapidly during the temperature. Then these peaks, representing the functional groups of C_{Ar}–H, –CH_2– and P–O–C_{Ar}, disappear slowly by slowly, while the peak, representing the functional group of CO_2, appears again and a new peak, representing the functional group of alkyne, appears at about 550 °C. All of these indicate that the first step is probably the process of thermal degradation, macromolecules being decomposed into micromolecules including many functional groups such as C_{Ar}–H, –CH_2–, –OH, P–O–C_{Ar}, and the second step probably the process of combustion, the layer of carbon being further oxidized into carbon dioxide, water and alkyne.

Figure 3c shows the peak area–temperature curves of some important functional groups (C_{Ar}–H, –CH_2–, P–O–C_{Ar}, alkyne and carbon dioxide) released in the process of the ABS/HMP degradation. The curve of the area of FTIR absorbance peak on functional groups such as C_{Ar}–H, –CH_2– and P–O–C_{Ar} begin arise quickly at about 367 °C, which is similar to the T_{1onset} (365 °C) shown in Table 2, and reach their only peaks at about 422 °C (T_{1max} 420 °C). The alkyne releases rapidly from 500 to 650 °C. There are two peaks for the release amounts of carbon dioxide from 350 to 677 °C. One peak is at 420 °C, and the other is at 571 °C, which is similar to the DTG (one peak at 420 and the other one at 589 °C). The semi-quantitative analyses of ABS/HMP indicate that the release of the gas is responding to the mass loss shown in DTG. At the same time, the semi-quantitative analyses further clarify the two-step process of degradation, the first one being thermal degradation and the second one being combustion.

FTIR analyses of ABS/HMP/NP

Figure 4a shows the three-dimensional (3D) FTIR spectrum for the gases produced during the thermal degradation of ABS/HMP/NP under air. Similar to ABS/HMP, most of the peaks appear at 35–45 min (400–500 °C), while several peaks appear at about 50 min (550 °C). Thus, ABS/HMP/NP decomposed in a two-step process, which also agrees with TG and DTG in Fig. 1.

Figure 4b shows the FTIR of ABS/HMP/NP at different temperatures under air. The curve of FTIR has few peaks before 350 °C, which indicates there is little decomposition before 350 °C. From 400 to 450 °C, there are a lot of peaks representing the functional groups of C_{Ar}–H, –CH_2–, P–O–C_{Ar}, P=O, CO_2, –OH and C=C, which indicates that the composite begins to decompose rapidly during the temperature. Then these peaks, representing the functional groups of C_{Ar}–H, –CH_2– and P–O–C_{Ar}, disappear slowly by slowly,
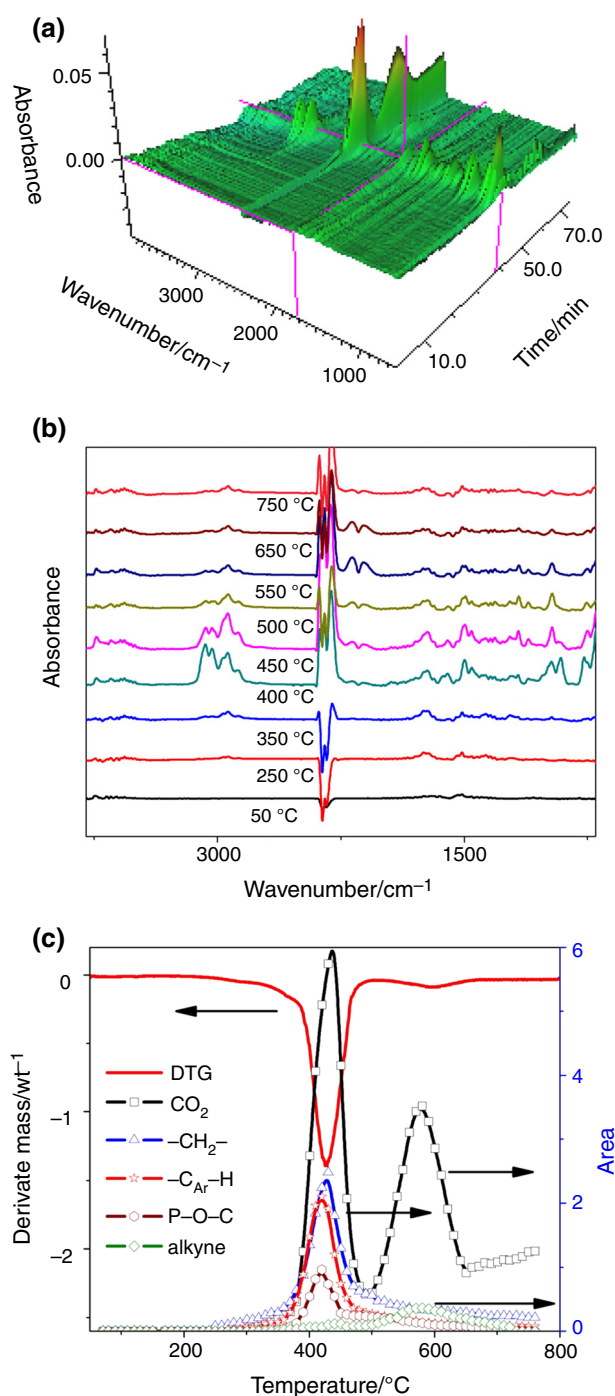
Fig. 4 FTIR spectra of ABS/HMP/NP (**a** three-dimensional diagram corresponding to gases evolved from degradation under air, **b** FTIR spectra of pyrolysis products of different temperatures under air and **c** functional group's peak area at different temperatures)

while the peak representing CO_2 appears again and a new peak, representing the functional group of alkyne, appears at about 550 °C. All of these indicate that the degradation of ABS/HMP/NP shown in Fig. 4 follows a similar trend to ABS/HMP shown in Fig. 3. The first step is probably the process of thermal degradation, macromolecules being

decomposed into micromolecules including many functional groups such as C_{Ar}–H, –CH_2–, –OH, P–O–C_{Ar}, and the second step probably the process of combustion, the layer of carbon being further oxidized into carbon dioxide, water and alkyne. There are differences between ABS/HMP/NP and ABS/HMP in the process of thermal decomposition. CO_2 is detected before 623 K, which indicates that the initial decomposition temperature of ABS/HMP is lower than that of ABS/HMP/NP. Besides, the peak strength of P–O–C_{Ar} for ABS/HMP/NP is weaker than that for ABS/HMP, which means that little gas containing P–O–C_{Ar} escapes in the process of thermal decomposition for ABS/HMP/NP.

Figure 4c shows the peak area–temperature curves of some important functional groups (C_{Ar}–H, –CH_2–, P–O–C_{Ar}, alkyne and carbon dioxide) released in the process of the ABS/HMP degradation. The curves of the area of FTIR absorbance peak on functional groups such as C_{Ar}–H, –CH_2– and P–O–C_{Ar} begin arise quickly at about 655 K, which is the same as the T_{1onset} (382 °C) shown in Table 2, and reach their only peak at about 432 °C (T_{1max} 426 °C). The alkyne releases rapidly from 500 to 650 °C. There are two peaks for the release amounts of carbon dioxide from 350 to 677 °C, and one peak is at 434 °C and the other is at 579 °C, which is similar to the DTG (one peak at 426 °C and the other one at 600 °C). The semi-quantitative analyses of ABS/HMP/NP indicate that the release of the gas is responding to the mass loss shown in DTG. At the same time, the semi-quantitative analyses further clarify the two-step process of degradation, the first one being thermal degradation and the second one being combustion.

FTIR analyses of ABS/NP

Figure 5a shows the three-dimensional (3D) FTIR spectrum for the gases produced during the thermal degradation of ABS/NP under air. Similar to ABS/HMP and ABS/HMP/NP, most of the peaks appear at 35–45 min (400–500 °C), while several peaks appear at about 53 min (580 °C). Thus, ABS/NP decomposes in a two-step process, which also agrees with TG and DTG in Fig. 1. But there are few peaks than ABS/HMP and ABS/HMP/NP.

Figure 5b shows the FTIR of ABS/NP at different temperatures under air. The curve of FTIR has few peaks before 350 °C, which indicates there is little decomposition before 350 °C. From 400 to 450 °C, there are a lot of peaks representing the functional groups of C_{Ar}–H, –CH_2–, CO_2 and –OH, which indicates that the composite begins to decompose rapidly during the temperature. Then these peaks, representing the functional groups of C_{Ar}–H and –CH_2–, disappear little by little, while the peak representing CO_2 appears again and a new peak, representing the functional group of alkyne, appears at about 550 °C. All of these indicate that the degradation
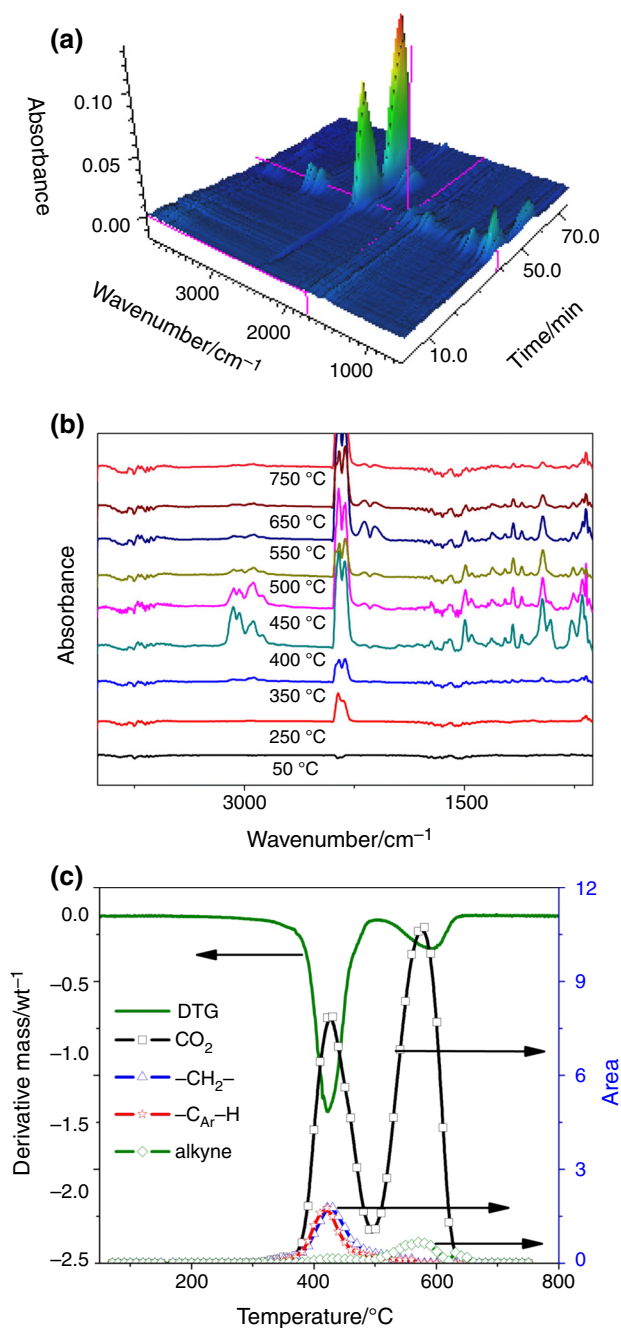

Fig. 5 FTIR spectra of ABS/NP (**a** FTIR spectra of pyrolysis products for different temperatures under air and **b** functional group's peak area at different temperatures and **c** three-dimensional diagram corresponding to gases evolved from degradation under air)

of ABS/NP shown in Fig. 5 follows a similar trend to ABS/HMP shown in Fig. 3 and ABS/HMP/NP shown in Fig. 4. The first step is probably the process of thermal degradation, macromolecules being decomposed into micromolecules including many functional groups such as C_{Ar}–H, –CH_2– and –OH, and the second step probably the process of combustion, the layer of carbon being further oxidized into carbon dioxide, water and alkyne.

Figure 5c shows the peak area–temperature curves of some important functional groups (C_{Ar}–H, –CH_2–, alkyne and carbon dioxide) released in the process of the ABS/NP degradation. The curve of the area of FTIR absorbance peak on functional groups such as C_{Ar}–H and –CH_2– begin arise quickly at about 377 °C, which is the same as the T_{1onset} (377 °C) shown in Table 2, and reach their only peak at about 427 °C (T_{1max} 422 °C). The alkyne releases rapidly from 500 to 650 °C. There are two peaks for the release amounts of carbon dioxide from 350 to 677 °C, and one peak is at 426 °C and the other one is at 574 °C, which is similar to the DTG (one peak at 422 °C and the other one at 595 °C). The semi-quantitative analyses of ABS/NP indicate that the release of the gas is responding to the mass loss shown in DTG. At the same time, the semi-quantitative analyses further clarify the two-step process of degradation, the first one being thermal degradation and the second one being combustion.

The comparison of the semi-quantitative analyses

The experimental conditions of the three samples are the same including the same instrument, the same air reservoir, and the time is consecutive. As a result, comparing the semi-quantitative analysis results of the three samples is reasonable.

The content of water in air bottle is invariable, and 3700–3750 cm^{-1} is O–H stretching vibration. The areas of water-peak are constantly changing before 100 °C, which is owing to that instrument operation instability and that the pipe, connecting the TG and FTIR, has water vapor. After 100 °C, the area of water-peak tends to be stable. As a result of that, there is a little mass loss as shown in TG curves in Fig. 1a after 100 °C and a small amount of decomposition; the area of water-peak after 100 °C cannot be chosen. Since the total water content is the same, the average value of the area from 50 to 100 °C can be introduced as shown in Fig. 6. Before 100 °C, the three compositions have no mass loss as shown in the TG curves in Fig. 1a. The areas of water-peak for ABS/HMP, ABS/HMP/NP, ABS/NP are 0.056, 0.070, 0.082, respectively.

Semi-quantitative analysis is based on Beer–Lambert law, and its mathematical expression is

$$A(v) = \ln \frac{I_0(v)}{I_t(v)} = \ln \frac{1}{T(v)} = K(v)LC. \tag{3.3.1}$$

$A(v)$, absorbance; $I_0(v)$, intensity of the incident light; $I_t(v)$, output optical intensity; $T(v)$, transmittance; $K(v)$, proportionality coefficient of light being absorbed; L, optical path length; C, sample concentration; $K(v)$, proportionality coefficient of light being absorbed.

For the gas, the above mathematical expression can be written as:

$$A(v) = K(v)PL \tag{3.3.2}$$

P, the partial pressure of the gas;

$$A(v) \propto P \tag{3.3.3}$$

Virial equation applies to all gas environments.

$$PV = nZRT \; (Z = 1 + B'P + C'P^2 + D'P^3 + \cdots) \,\text{(Virial equation)};$$

$$n = \frac{PV}{RTZ}; \quad n \propto \frac{A(v)V}{RTZ}; \quad n \propto \frac{A_T(v)}{A_0(v)TZ} \tag{3.3.4}$$

n, amount of substance; R, perfect gas equation (constancy); T, temperature; V, volume (constancy); B', C', D'…, virial coefficient (function on T).

Compared with the air going into the equipment, the gas generation in the degradation process can be ignored. So Z is the function of T.

$A(v)$ needs to be corrected. The average value of the area for the three samples from 323 K to 373 K can be expressed as A_0 (ABS/HMP 0.056, ABS/HMP/NP 0.070 and ABS/NP 0.082).

$$A(v) = \frac{A_T(v)}{A_0(v)}; \quad n = \frac{A_T(v)V}{A_0(v)RTZ}; \tag{3.3.5}$$

To clear the conversion ratio of unit mass of element or functional groups into the corresponding gas, the content of the element or functional groups for every sample should be known from Table 4.

$$a = \frac{nM}{mw} \tag{3.3.6}$$

α, conversion ratio; M, molar mass of the corresponding molecule; m, the mass of the sample; w, the content of the element or functional groups for every sample.

Thus, there exists the expression

$$a = k(T) \frac{A_T(v)}{A_0(v)mw} \tag{3.3.7}$$

k, correction factor (function on T).

The rise rates of temperature for the three samples are the same and will not affect the comparison of their conversion rate at the same temperature. So the Y-axis can use αk^{-1} to compare their conversion rate.

Figure 6a shows the conversion ratio of the element of C into CO_2 with the temperature increasing. The variation tendency of the conversion ratio for ABS/HMP/NP is similar to that for ABS/HMP and ABS/NP. The conversion ratios of the these three samples arise quickly at about 377 °C and reach their first maximum (ABS/HMP at 420 °C, ABS/HMP/NP at 434 °C and ABS/NP at 426 °C as
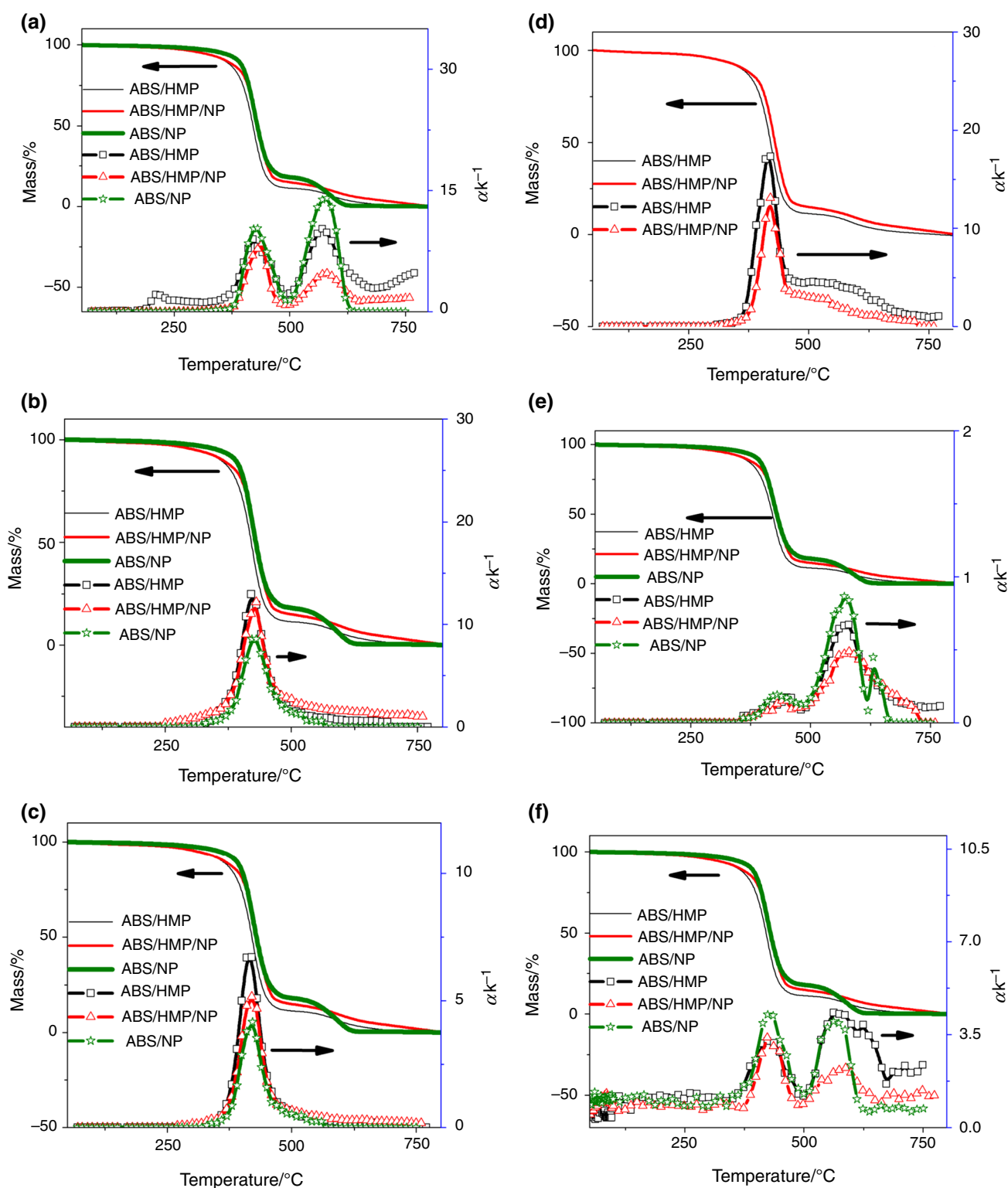
Fig. 6 Conversion ratio of different functional groups or elements with the variation of temperatures (**a** CO_2; **b** $-CH_2-$; **c** $-C_{Ar}-H-$; **d** $P-O-C_{Ar}$; **e** alkyne; **f** H_2O)

shown in Table 5), then decline rapidly, and go up quickly at about 500 °C until clamp their second maximum (ABS/HMP at 571 °C, ABS/HMP/NP at 579 °C and ABS/NP at

574 °C as shown in Table 5). The conversion ratios of three samples agree with their TG curves. From 377 to 477 °C, the conversion ratio of the element of C into CO_2 for ABS/

Table 4 Content of the element or functional groups

Sample	Components/mass%				
	C	H	P–O–C_{Ar}	–CH_2–	C_Ar–H
ABS/HMP	76.9	7.5	11.8	21.2	42.4
ABS/HMP/NP	79.1	7.9	7.87	21.7	43.6
ABS/NP	83.5	8.5	\	22.5	46.0

Table 5 Temperature at different functional groups' maximal conversion ratio

Functional group	Sample ID	T_{1max}/°C	T_{2max}/°C
CO_2	ABS/HMP	420	571
	ABS/HMP/NP	434	579
	ABS/NP	426	574
–CH_2–	ABS/HMP	421	\
	ABS/HMP/NP	427	\
	ABS/NP	425	\
C_{Ar}–H	ABS/HMP	414	\
	ABS/HMP/NP	420	\
	ABS/NP	418	\
P–O–C	ABS/HMP	414	\
	ABS/HMP/NP	420	\
	ABS/NP	\	\
Alkyne	ABS/HMP	\	571
	ABS/HMP/NP	\	579
	ABS/NP	\	574
H_2O	ABS/HMP	422	569
	ABS/HMP/NP	424	586
	ABS/NP	426	565

NP is a little higher than that for ABS/HMP and ABS/HMP/NP. From 577 to 627 °C, the conversion ratio for ABS/NP much higher than that for ABS/HMP and the conversion ratio for ABS/HMP/NP is the least, which is corresponding to the TG curves. This is probably because ABS/HMP and ABS/HMP/NP form tight layer of carbon under the action of phosphoric acid. Figure 6b shows the conversion ratio of the functional group of –CH_2– in solid phase into –CH_2– in gas phase with the temperature increasing. The conversion ratios of the three samples arise quickly at about 377 °C and reach their maximum (ABS/HMP at 421 °C, ABS/HMP/NP at 427 °C and ABS/NP at 425 °C as shown in Table 5). The conversion ratios of three samples agree with their TG curves. The conversion ratio for ABS/HMP is the highest, while the conversion ratio for ABS/NP is the lowest, which is probably due to the functional group of –OH from NP absorbing the functional group of –CH_2– in the first degradation step. Figure 6c shows the conversion ratio of the functional group of C_{Ar}–H in solid phase into C_{Ar}–H in

gas phase with the temperature increasing. The conversion ratios of three samples arise quickly at about 377 °C and reach their maximum (ABS/HMP at 414 °C, ABS/HMP/NP at 420 °C and ABS/NP at 418 °C as shown in Table 5). The conversion ratios of three samples agree with their TG curves. From 377 to 477 °C, the conversion ratio for ABS/HMP is the highest, while the conversion ratio for ABS/NP is the lowest, which is probably owing to –OH from NP absorbing the functional group of C_{Ar}–H in the first degradation step. Figure 6d shows the conversion ratio of the functional group of P–O–C_{Ar} in solid phase into P–O–C_{Ar} in gas phase with the temperature increasing. The conversion ratios of ABS/HMP and ABS/HMP/NP arise quickly at about 377 °C and reach their maximum (ABS/HMP at 414 °C and ABS/HMP/NP at 420 °C). The conversion ratio of ABS/HMP and ABS/HMP/NP agrees with their TG curves. ABS/HMP/NP has no functional group of P–O–C_{Ar}. The conversion ratio for ABS/HMP/NP is slower than that for ABS/HMP, which is probably attributed to –OH from NP which can absorb O=P–OH in the first degradation step. Figure 6e shows the conversion ratio of the element of C into alkyne with the temperature increasing. The conversion ratios of the three samples arise quickly at about 800 K and reach their maximum (ABS/HMP at 571 °C, ABS/HMP/NP at 579 °C and ABS/NP at 574 °C as shown in Table 5). The conversion ratios of the three samples agree with their TG curves. From 527 to 627 °C, the conversion ratio for ABS/NP is highest, while the conversion ratio for ABS/HMP/NP is the lowest, which is probably ascribed to the protection from phosphoric-oxygenic compound in the second degradation step. Figure 6f shows the conversion ratio of the element of H in solid phase into H_2O in gas phase with the temperature increasing. The conversion ratios of the three samples arise quickly about 650 K and reach their first maximum (ABS/HMP at 422 °C, ABS/HMP/NP at 424 °C and ABS/NP at 426 °C as shown in Table 5), then decline rapidly, and go up quickly at about 500 °C until clamp their second maximum (ABS/HMP at 569 °C, ABS/HMP/NP at 586 °C and ABS/NP at 565 °C). The conversion ratios of the three samples agree with their TG curves. From 377 to 477 °C, as the first degradation step, the conversion ratio of the element of H in solid phase into H_2O in gas phase for ABS/NP is a little higher than that for ABS/HMP/NP and ABS/HMP, which is probably owing to the functional group of –OH from NP which absorbs the functional group of –OH, C_{Ar}–H and –CH_2– generating in the first degradation step. From 500 to 627 °C, in the second degradation step, the conversion ratio of the element of H in solid phase into H_2O in gas phase for ABS/NP declines quickly at 588 °C, while the other two samples do not experience this kind of situation. Meanwhile, from 577 to 627 °C, the conversion ratios of H for ABS/NP and ABS/HMP are much higher than that for ABS/
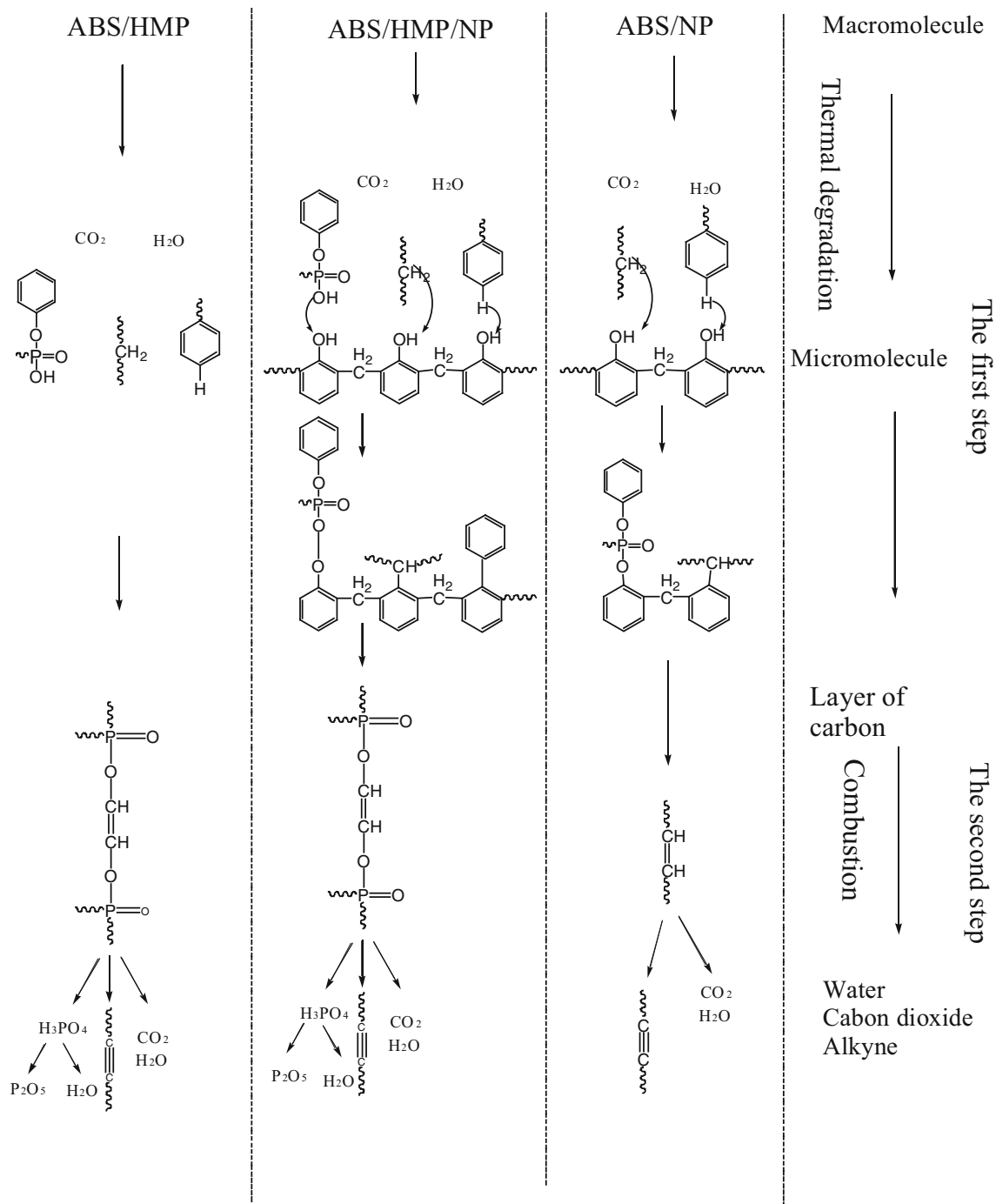
Fig. 7 Possible mechanism of ABS/HMP, ABS/HMP/NP and ABS/NP

HMP/NP. This is probably because of the protection of carbon layers and phosphoric-oxygenic compound.

All of these pictures in Fig. 6 show that NP can absorb parts of –OH, C_{Ar}–H and –CH_2– generating in the first degradation step, contributing to the formation of the layer of carbon in the first degradation step [30, 31], and HMP slows down the degradation of the layer of carbon in the second degradation step, achieving the cooperative effect.

Possible mechanism

Based on the analyses mentioned above, it is concluded that the degradation of ABS/HMP/NP has two steps as shown in Fig. 7. In the first step, macromolecules are decomposed into micromolecules containing many functional groups such as C_{Ar}–H, –CH_2–, –OH, P–O–C_{Ar}, and parts of the micromolecules are oxidized into CO_2 and H_2O. In this process, parts

of micromolecules containing functional groups of C_{Ar}–H, –CH_2– and –OH are absorbed by the functional group from NP and generate H_2O, which is in favor of the formation of the layer of carbon and dilute the surrounding air [27]. In the second step, with the increase in temperature, the layer of carbon is oxidized slowly with the protection of phosphoric-oxygenic compound. It is probably that P–O–C, generating in the degradation process, protects the layer of carbon from being oxidized in the second degradation process. In the end, the composition of ABS/HMP/NP is decomposed into carbon dioxide, alkyne and phosphoric acid [14, 32], and phosphoric acid is decomposed into P_2O_5 [33].

Conclusions

In this study, the thermal degradation behavior of ABS/HMP, ABS/HMP/NP and ABS/NP is investigated under air based on TG–FTIR analyses. The TG and DTG results indicate that all of three samples decompose via a two-step process. The FTIR analyses demonstrate that the composites are decomposed into micromolecules containing many functional groups such as C_{Ar}–H, –CH_2–, –OH, P–O–C_{Ar} in the first step, whereas the second step is mainly the further oxidization into carbon dioxide and alkyne. The results, comparing the conversion ratio of the functional groups of C_{Ar}–H, –CH_2–, P–O–C_{Ar} with the variation of temperatures for the three samples, demonstrate that the functional group of –OH from NP can absorb parts of micromolecules containing the functional group of –OH, C_{Ar}–H and –CH_2–, contributing to the formation of the layer of carbon. The results, comparing the conversion ratio of the functional groups of carbon dioxide and alkyne with the variation of temperatures for the three samples, demonstrate that HMP can slow down the degradation of the layer of carbon. The cooperative effect of HMP and NP exists in ABS.

References

1. Zhang Y, Chen XL, Fang ZP. Synergistic effects of expandable graphite and ammonium polyphosphate with a new carbon source derived from biomass in flame retardant ABS. J Appl Polym Sci. 2013;128:2424–32.
2. Yin HQ, Yuan DD, Cai XF. The high efficiency two stage intumescent-contractive flame retardant on ABS. Polym Degrad Stabil. 2013;98:288–96.
3. Ren YY, Chen L, Zhang ZY, Wang XL, Yang XS, KongXJ Yang L. Synergistic effect of hydroquinone bis(di-2-methylphenyl phosphate) and novolac phenol in ABS composites. Polym Degrad Stabil. 2014;109:285–92.
4. Suzuki M, Wilkie CA. The thermal degradation of acrylonitrile-butadiene-styrene terpolymei as studied by TG/FTIR. Polym Degrad Stabil. 1995;47:217–21.
5. Wang SF, Hu Y, Zong RW, Tang Y, Chen ZY, Fan WC. Preparation and characterization of flame retardant ABS/montmorillonite nanocomposite. Appl Clay Sci. 2004;25:49–55.
6. Ji YY, Kim JH, Bae JY. Flame-retardant ABS resins from novel phenyl isocyanate blocked novolac phenols and triphenyl phosphate. J Appl Polym Sci. 2006;102:721–8.
7. Akbar NQ, Hossein RM, Mehdi SK. Novolac phenolic resin and graphene aerogel organic-inorganic nanohybrids: High carbon yields by resin modification and its incorporation into aerogel network. Polym Degrad Stabil. 2016;124:1–14.
8. Costa L, Montelera L, Camino G, Weil ED, Pearce EM. Flame-retardant properties of phenol–formaldehyde-type resins and triphenyl phosphate in styrene–acrylonitrile copolymers. J Appl Polym Sci. 1998;68:1067–76.
9. Murashko EA, Levchik GF, Levchik SV, Bright DA, Dashevsky S. Fire-retardant action of resorcinol bis(diphenyl phosphate) in PCeABS blend: II: reactions in the condensed phase. J Appl Polym Sci. 1999;71:1863.
10. Danielle AB, Sophia D, Paul YM, Barbara W. Resorcinol bis(diphenyl phosphate), a non-halogen flame-retardant additive. J Vinyl Addit Technol. 1997;3:170.
11. Kristin HP, Bernhard S, Mario AF, Christian J. Flame retardancy mechanisms of bisphenol A bis(diphenyl phosphate) in combination with zinc borate in bisphenol A polycarbonate/acrylonitrileebutadieneestyrene blends. Thermochim Acta. 2010;498:92.
12. Ma HY, Tong LF, Xu ZB, Fang ZP, Jin YM, Lu FZ. A novel intumescent flame retardant: synthesis and application in ABS copolymer. Polym Degrad Stab. 2007;92:720.
13. Fu QJ, Wang XL, Zhang ZY, Zhou J, Li JX, Zhong BH, et al. Synthesis of phosphorus flame retardant HDP in a novel process and its role in ABS composites. Acta Polym Sin. 2013;2:154.
14. Chen L, Yang ZY, Ren YY, Zhang ZY, Wang XL, Yang XS, Yang L, Zhong BH. Fourier transform infrared spectroscopy-thermogravimetry analyses of the thermal decomposition mechanism of an effective flame retardant, hydroquinone bis(di-2-methylphenyl phosphate). Polym Bull. 2015;73:927–39.
15. Jong W, Pirone A, Wójtowicz MA. Pyrolysis of *Miscanthus giganteus* and wood pellets: TG-FTIR analyses and reaction kinetics. Fuel. 2003;82:1139–47.
16. Kanokkantapong V, Marhaba TF, Panyapinyophol B, Pavasant P. FTIR evaluation of functional groups involved in the formation of haloacetic acids during the chlorination of raw water. J Hazard Mater. 2006;136:188–96.
17. Becidan M, Skreiberg Y, Hustad E. Products distribution and gas release in pyrolysis of thermally thick biomass residues samples. J Anal Appl Pyrol. 2007;78:207–13.
18. Wójtowicz MA, Bassilakis R, Smith WW, Chen YG, Carangelo RM. Modeling the evolution of volatile species during tobacco pyrolysis. J Anal Appl Pyrol. 2003;66:235–61.
19. Herrera M, Wilhelm M, Matuschek G, Kettrup A. Thermoanalytical and pyrolysis studies of nitrogen containing polymers. J Anal Appl Pyrol. 2001;58–59:173–88.
20. Fernández-Berridi MJ, González N, Mugica A, Bernicot C. Pyrolysis-FTIR and TG techniques as tools in the characterization of blends of natural rubber and SBR. Thermochim Acta. 2006;444:65–70.
21. Dong D, Tasaka S, Aikawa S, Kamiya S, Inagaki N, Inoue Y. Thermal degradation of acrylonitrile–butadiene–styrene terpolymer in bean oil. Polym Degrad Stabil. 2001;73:319–26.
22. Liu Y, Zhao XR, Peng YL, Wang D, Yang LW, Peng H, Zhu P, Wang DY. Effect of reactive time on flame retardancy and thermal degradation behavior of bio-based zinc alginate film. Polym Degrad Stabil. 2015;127:20–31.

23. Liu Y, Zhao J, Zheng CJ, Cui L, Guo Y, Zhu P, Zhang H, Zheng ZW, Wang DY. Flame retardancy and thermal degradation properties of cotton/alginate fabric. J Therm Anal Calorim. 2016;. doi:10.1007/s10973-016-5418-6.

24. Zheng ZH, Liu Y, Zhang L, Dai B, Yang XD, Wang HY. A Fabrication of halogen-free ammonium phosphate with two components via a simple method and its flame retardancy in polypropylene composites. J Therm Anal Calorim. 2016;. doi:10.1007/s10973-016-5779-x.

25. Chen XL, Ma CY, Jiao CM. Synergistic effects between iron-graphene and ammonium polyphosphate in flame-retardant thermoplastic polyurethane. J Therm Anal Calorim. 2016;126: 633–42.

26. Yang S, Wang J, Huo SQ, Wang JP, Tang YS. Synthesis of a phosphorus/nitrogen-containing compound based on maleimide and cyclotriphosphazene and its flame-retardant mechanism on epoxy resin. Polym Degrad Stabil. 2016;126:9–16.

27. Lee K, Yoon K, Kim J, Bae J, Yang J, Hong S. Effect of novolac phenol and oligomeric aryl phosphate mixtures on flame retardance enhancement of ABS. Polym Degrad Stabil. 2003;81: 173–9.

28. Jin CW, Shen PP, Ren N, Geng LN, Zhang JJ. Structure, luminescent and thermal properties of two novel lanthanide complexes with 3,4-diethoxybenzoic acid and 5,50-dimethy-2,20-bipyridine. J Therm Anal Calorim. 2016;126:1549–58.

29. Wang S, Hu Y, Wang Q, Xu S, Lin X, Ji H, Zhang Z. TG–FTIR–MS analysis of the pyrolysis of blended seaweed and rice husk. J Therm Anal Calorim. 2016;126:1689–702.

30. Haddadi SA, Kardar P, Abbasi F, Mahdavian M. Effects of nano-silica and boron carbide on the curing kinetics. J Therm Anal Calorim. 2016;. doi:10.1007/s10973-016-5951-3.

31. Noparvar-Qarebagh A, Roghani-Mamaqani H, Salami-Kalajahi M, Kariminejad B. Effects of nano-silica and boron carbide on the curing kinetics of resole resin. J Therm Anal Calorim. 2016;. doi:10.1007/s10973-016-5970-0.

32. Laoutid F, Bonnaud L, Alexandre M, Lopez-Cuesta J-M, Dubois P. New prospects in flame retardant polymer materials: From fundamentals to nanocomposites. Mater Sci Eng, R. 2009;63:100–25.

33. Jiang WZ, Hao JW, Han ZD. Study on the thermal degradation of mixtures of ammonium polyphosphate and a novel caged bicyclic phosphate and their flame retardant effect in polypropylene. Polym Degrad Stab. 2012;97:632–7.